Journal of Applied Polymer Science

Improved gas selectivity of polyetherimide membrane by the incorporation of PIM polyimide phase

María G. García, José Marchese, Nelio A. Ochoa
Instituto de Física Aplicada CONICET-Universidad Nacional de San Luis, Chacabuco 917, San Luis, CP 5700, Argentina
Correspondence to: M. G. García (E-mail: maggarcia@unsl.edu.ar)

ABSTRACT: The aim of this work was to prepare blend membranes of a polyetherimide (PEI) and different ratios of a microporous polyimide (PIM-B) in order to obtain an improved material for gas selectivity. Miscibility of the membranes was studied through fourier transform infrared spectroscopy (FTIR), Fluorescence, ultraviolet-visible spectroscopy (UV–vis), polarize light microscope images, x-ray diffraction (XRD), and differential scanning calorimetry analysis. Gas permeability assays were also performed. Results showed blends were partially miscible along the different ratios due to the existence of: (i) absorption shoulders at lower wavenumbers on the carbonyl stretching band; (ii) red-shifting of Fluorescence and UV–vis absorption bands; (iii) decreasing of d-spacing as the amount of PIM-B phase increased; and (iv) composition-dependent glass transition temperatures (T_{gs}). The mobility selectivity ($D_{i/j}$) dominated H_2 and O_2 gas separations. High solubility coefficients (S) linked to PIM-B microporosity improved the ideal gas selectivity of the blend membranes. PEI/PIM-B membrane at the ratio of 80/20 showed impressive H_2/CO_2 (8.66) and O_2/N_2 (10.90) gas separation factors. © 2016 Wiley Periodicals, Inc. J. Appl. Polym. Sci. **2016**, *134*, 44682.

KEYWORDS: blends; differential scanning calorimetry; membranes; polyimides; X-ray

Received 21 June 2016; accepted 15 November 2016
DOI: 10.1002/app.44682

INTRODUCTION

New polymeric materials are synthesized and modified in order to achieve a profitable combination of permeability and selectivity that surpasses Robeson's limit.[1,2] Nowadays, the synthesis of new polymers from suitable monomers to produce selective membranes has been restricted due to time and cost. An alternative way for the development of new polymeric materials is the polymer blending. Polymer blends are able to yield property profiles superior to those of individual components. In addition, polymer blends can be tailored by combining different polymers and changing the blend composition. Nevertheless, polymer blend membranes possess several drawbacks related to miscibility and homogeneity of blend components.[3–9] Numerous research works have demonstrated that a large number of polymers with appropriate functional groups can form interassociation such as hydrogen bonds (H-bond) and charge transfer complex (CTC) that enhance compatibility of immiscible blends.[3,4] H-bonding as well as CTC can take place intra- or intermolecularly. In both cases, at least two different functional groups have to be present in polymers. For years, a number of novel polymer blends based on polyimides (PIs) have been developed and used in diverse fields. PIs demonstrated to be miscible with glassy polymers such as polybenzimidazole (PBI),[10] polyetheretherketone (PEEK),[11] polyethersulfone (PES),[12,13] sulfonated PEEK,[14] polyetherimide (PEI),[15,16] among others.[17,18] Nevertheless, there are few data reported about gas transport properties of blends comprising glassy and microporous polymers. Polymers of intrinsic microporosity (PIMs) feature porosity derived from inefficient packing due to the combination of rigid segments and sites of contortion (stiff units with spiro-center) within the macromolecular backbone of the polymer.[19–22] These characteristics render polymers with high fractional free volumes (FFV) and rigid backbones that might perform high permeabilities and low-to-moderate selectivities in gas separation applications.[23–28] Thus, small and nonpolar gas molecules such as hydrogen (H_2) might permeate easily through microporosity, while bigger and polar gas molecules such as carbon dioxide (CO_2) may be retarded in the polymer matrix. Only two recent studies conducted by Chung *et al.*[1,29] showed the performance of PIM-1/Matrimid and Ultem/PIM-1 blend membranes for gas separation. These authors found that blending a polymer of intrinsic microporosity with a glassy polymer caused a significant increase in gas permeability with a moderate to high decrease in gas-pair selectivity depending on the polymers ratio. The aim of this

Additional Supporting Information may be found in the online version of this article.

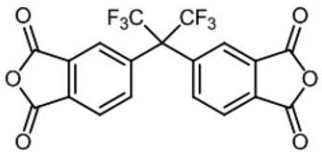

4, 4'- (Hexafluoroisopropylidene) diphthalic anhydride (6FDA)

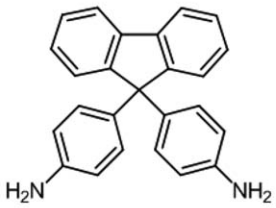

4, 4'- (9-Fluorenylidene) dianiline (9FDA)

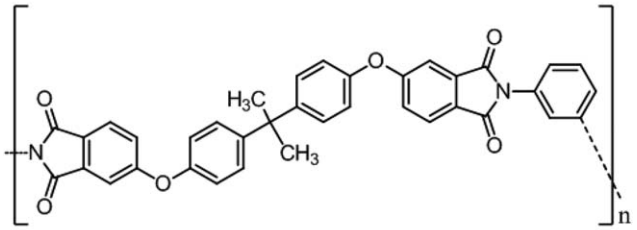

Polyetherimide (PEI, ULTEM 1000)

Figure 1. Chemical structure of monomers and polyetherimide.

work is to prepare blend membranes from a glassy polymer (PEI) and different ratios (10, 20, and 50 wt %) of a polymer of intrinsic microporosity (PIM-B) in order to improve gas selectivity. PEI is a commercially available high-performance, high-temperature engineering thermoplastic, which is miscible with a variety of aromatic polymers.[30–35] PIM-B is an already synthesized microporous polyimide, which depicted surface areas of $S_{AH2} = 301$ and $S_{ACO2} = 221$ m^2 g^{-1}.[36] H_2, N_2, O_2, CH_4, and CO_2 gas permeabilities were measured using a "time lag" apparatus. The solution-diffusion model was used to discuss the mechanism of gas transport in the membranes.

EXPERIMENTAL

Materials

Monomers for the synthesis of PIM-B were supplied by Sigma-Aldrich and purified by vacuum sublimation: 4,4′-(Hexafluoroisopropylidene) diphthalic anhydride (6FDA) and 4,4′-(9-Fluorenylidene) dianiline (9FDA). Benzoic Acid (Merck) was used as catalyst of imidization reactions without further purification. *N*,*N*-dimethylacetamide (DMAc, Sigma-Aldrich) and dichloromethane (DCM, Sigma-Aldrich) were used as solvents. General Electric provided Polyetherimide Ultem 1000 (PEI) that was used as received. Pure gases for the permeation study were hydrogen, nitrogen, oxygen, methane, and carbon dioxide, since they provide information about several industrially pertinent separations, such as air (O_2/N_2), natural gas (CO_2/CH_4), and hydrogen purifications like in water gas shift (WGS) reactions (H_2/CO_2). Air Liquid (Argentina) supplied all gases and their purities were more than 99.95%. Figure 1 shows the chemical structure of monomers and PEI.

Synthesis of PIM and Preparation of Blends

Polyimide of intrinsic microporosity (PIM-B) was synthesized in a one-step synthesis using Benzoic acid as catalyst and DMAc as solvent. First, an adequate amount of diamine (0.1743 g, 0.5 mmol of 9FDA) was dissolved in DMAc (15 mL) at ambient temperature, N_2 atmosphere and constant stirring. Then, an equimolar amount of the dianhydride (0.2222 g, 0.5 mmol of 6FDA) was added under agitation. After 10 min, 2 mmol of benzoic acid were incorporated into the reaction mixture and stirred for 2 h. After that, the temperature was raised to 80 °C and held overnight. Finally, the temperature was raised to 180 °C and held for 3 h in order to obtain the polyimide solution. PIM-B solution was precipitated in methanol and washed several times with this solvent in order to remove any residue of benzoic acid. Then, the precipitate was dried in a vacuum oven at 120 °C. Weight–average molecular weight (M_w) and number–average molecular weight (M_n) of synthesized PIM-B were measured on gel permeation chromatography (GPC) (polyethylene oxide calibration) using a Phenogel Column attached to a Gilson HPLC with DMAc as mobile phase. M_w, M_n, and polydispersity (PDI M_w/M_n) were 26,000, 18,000, and 1.47, respectively. Two different solvents were proved to prepare PIM-B films. Thus, PIM-B-DCM and PIM-B-$CHCl_3$ solutions were casted onto flat glass plates covered by a lid to allow slow evaporation of the solvent at 30 °C overnight. Finally, the solvent was further eliminated under vacuum at 120 °C for 10 h. In both cases, PIM-B films exhibited low mechanical flexibility. PEI/PIM-B blends were prepared by introducing an adequate amount of PIM-B (10, 20, and 50 wt % with respect to PEI) in a PEI-DCM solution at ambient temperature and constant stirring. Then, each polymer solution was spread on a flat glass plate covered by a lid to allow slow evaporation of the solvent and the membrane was obtained by the solvent evaporation method. Finally, the obtained polymer membranes were further dried in an oven at 120 °C for 10 h. Blend membranes were called 90/10; 80/20; and 50/50 for PEI/PIM-B ratios, respectively, and they exhibited thicknesses in the range of 80 ± 5 μm.

Characterization Methods

FTIR Analysis. Fourier transform infrared spectroscopy (FTIR) spectra were determined by the diffuse reflectance (DRIFTS) mode using Nicolet PROTEGE 460 Spectrometer over the range of 400–4000 cm^{-1}. The number of scans for each sample was 64.

Fluorescence Spectroscopy. Fluorescence spectra were measured using a Shimadzu RF-5301 PC spectrofluorophotometer (Shimadzu Corporation, Analytical Instrument Division, Kyoto Japan) equipped with a 150 W Xenon lamp and a holder for solid films. Emission intensities were normalized with the membrane thickness measured with a Köfer micrometer (precision ±1 μm).

UV–Vis Spectroscopy. Ultraviolet-visible spectroscopy (UV–vis) spectra of PEI/PIM-B membranes were recorded on UV–vis U-

2001 Hitachi spectrophotometer over the wavelength range 200–700 nm. Absorption intensities were normalized with the membrane thickness measured with a Köfer micrometer (precision ±1 μm). Measurements were performed at ambient conditions.

Optical Properties. Optical appearance of PEI, PIM-B, and blend membranes was evaluated through the measurement of opacity (OP) and colorimetric parameters. Film opacity was determined through two different methods. First, according to ASTM D1003 recommendations[37] and second, using a Colorimeter MiniScan EZ model MSEZ-4500 L equipped with light source D65 and observation angle 10°. Each experiment was performed at least three times, and data was reported as the means of these values.

Polarize Light Microscope. Surface images of PEI, PIM-B, and blend membranes were obtained by an Olympus SZ51 Polarized Light Microscope (PLM) in order to further evaluate the miscibility of the blends. Images were then analyzed with ScanPro image software.

X-ray Diffraction. Wide-angle X ray diffraction (WAXD) measurements were carried out using a Rigaku model D-Max III C device, lamp of Cu-K (alpha) and filter of Nickel in a range of 2θ between 5° and 60°. From diffractograms, d-spacing of each membrane, defined as center-to-center space of polymer chains, were determined by Bragg's equation [Eq. (1)].

$$n\lambda = 2\ d\ \sin\ \theta \tag{1}$$

Diffraction patterns were normalized with the membrane thickness measured with a Köfer micrometer (precision ±1 μm). Measurements were performed at ambient conditions.

Differential Scanning Calorimetry. Differential scanning calorimetry (DSC) was performed to estimate the glass transition temperature (T_g) and the miscibility of polymer blends. DSC measurements were recorded on Shimadzu DSC-60. Operating conditions were as follows: (a) heating rate: 10 °C min^{-1} and, (b) atmosphere: dynamic N_2 (99.99%, flow rate 50 mL min^{-1}). Empty aluminum pans (40 mL) were used as references. Reported DSC values were the average of at least two independent measurements and reported data were processed with Thermal Solutions software (TA Instrument, Inc.).

Gas Permeation. Permeability was measured at 35 °C and 5 bar using a classical time lag apparatus.[38,39] The effective membrane area was 11.34 cm^2 and permeate constant volume was 35.37 cm^3. Gas permeation measurements were carried out after membrane degassed procedure consisting in high vacuum ($p \approx 10^{-4}$ torr) at $T = 80$ °C during 10 h. The amount of gas transmitted at time t through the membrane was calculated from the permeate pressure (p_2) readings in the low-pressure side of permeation cell. Permeability coefficients (P) were obtained from the flow rate into the downstream volume upon reaching the steady state as:

$$P = \frac{B\,l}{T_c\,p_1}\frac{dp_2}{dt} \tag{2}$$

where the cell constant $B = 11.53$ (cm^3(STP) K)/(cm^2 cmHg); high-pressure side p_1 (cmHg); membrane thickness l (cm), slope of the p_2 vs. t plot in steady state dp_2/dt (cmHg/s), temperature of the permeation cell T_c (K). Linear regression of p_2 vs. t allows determining the time elapsed until the steady state conditions have been reached. This "time lag" value (t_ℓ), can be evaluated from abscise axis at $p_2 = 0$ and it is related to the membrane thickness and diffusion coefficient (D) according to:

$$t_\ell = \frac{l^2}{6D} \tag{3}$$

Theoretical separation factors (α) were calculated from the relation between the permeation coefficients of pure i and j gases as:

$$\alpha_{i/j} = \frac{P_i}{P_j} \tag{4}$$

RESULTS AND DISCUSSION

Reaction Yield and Solubility

Polyimide reaction yields were above 80%. The solubility of PIM-B was tested qualitatively with different solvents such as: *N,N*-dimethylacetamide (DMAc), *N,N*-dimethylformamide (DMF), *N*-methyl-2-pirrolidinone (NMP), chloroform ($CHCl_3$), dichloromethane (DCM), and tetrahydrofuran (THF). PIM-B was soluble in all tested solvent at room temperature.

FTIR Analysis

IR spectra of PEI and blends were performed in order to verify the presence of imide bands and possible interaction between polymers blended at different ratios. Figure 2 and Table I show IR band assignments for all prepared membranes. PEI showed bands at 1778 and 1726 cm^{-1} attributed to asymmetric and symmetric stretch of imide carbonyl group, respectively. Besides, a band at 1356 cm^{-1} was attributed to C—N stretch of imide groups. PIM-B depicted same imide bands at 1784, 1722, and 1373 cm^{-1}, respectively. Those bands evidenced that complete imidization was achieved for PIM-B. Additionally, Figure S1, Supporting Information shows FTIR spectra of PEI, PIM-B and blend membranes in the region from 4000 to 2000 cm^{-1} in order to prove the complete imidization. FTIR spectra of Blend membranes also showed characteristic polyimide bands. Interestingly, the main carbonyl stretching band for all blend membranes shows the appearance of absorption contributions at lower wavenumbers, known as absorption shoulders. Absorption shoulders on a main FTIR band depict that the group identified at that wavenumber is being involved in some new kind of interaction that makes the energy necessary to exited the group is reduced, because the original bond strength is being weakened by the new interaction. This is the reason why 90/10, 80/20, and 50/50 blend membranes show absorption shoulders at 1716, 1718, and 1726 cm^{-1}, respectively. It is also observed that as the amount of PIM-B phase increases in the blend, the shoulder become more intense, meaning that more carbonyl groups are being involved in new intermolecular interactions. In case of 50/50 blend membrane, the intensity of the shoulder is much longer than that of the original carbonyl band which is identified at 1737 cm^{-1}. These absorption shoulders on the symmetric stretch band of carbonyl were attributed to the formation of weak intermolecular CTC interactions as the amount of PIM-B increased, which might be responsible for increasing

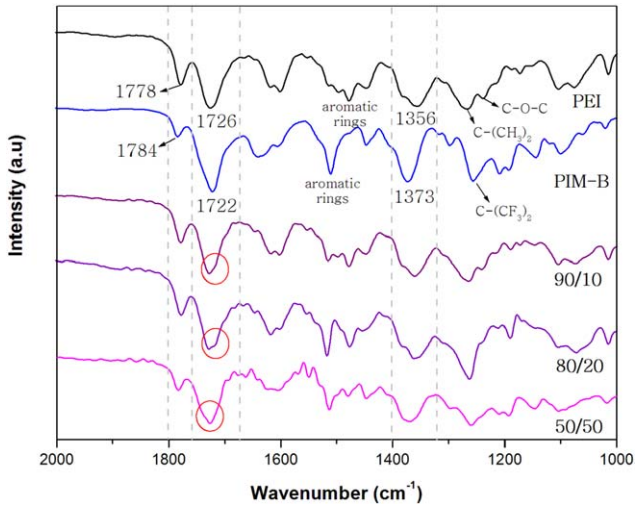

Figure 2. FTIR of PEI, PIM-B and the blend membranes. [Color figure can be viewed at wileyonlinelibrary.com]

miscibility in the blends.[40–42] Figure S2, Supporting Information shows absorption shoulders with more detail.

Besides, blend membranes showed a shift of the C—N stretching of the imide ring from 1360 to 1369 cm^{-1} as the amount of microporous polyimide increases. Shifting of C—N bands towards higher wavenumbers is attributed to the reduction of C—N bond length as a result of the strain induced in the imide ring due to the involvement of imide carbonyl in CTC. Similar C—N shift was observed for Carturan *et al.*[43] who studied the formation of intermolecular interaction, such as H-bonding, in a fluorinated polyimide. FTIR results were then confirmed by fluorescence and UV–vis analysis of polyimide blend membranes.

Fluorescent Properties

It may be expected that two different PIs having electron-donor and electron-acceptor in their chains, respectively, forms intermolecular charge-transfer complexes (CTC).[4] If polymer solutions are analyzed, an enhancement of fluorescence due to the aggregation of molecular chains is expected. On the contrary, if solid state polymers are analyzed it is well known that the densest molecular packing shows the weakest fluorescent intensity due to the intimate contact between the adjacent polymer chains.[44] These observations remark that the charge-transfer fluorescence in polyimides is not only related to the molecular aggregation, but also it is sensitive to the orientation of local

Table I. IR and UV–Vis Absorption Bands of Membranes

Polymer	C=O_{asy} (cm^{-1})	C=O_{sy} (cm^{-1})	Shoulder (cm^{-1})	C—N (cm^{-1})	λ (nm)
PEI	1778	1726	—	1356	255
PIM-B	1784	1722	—	1373	244
90/10	1778	1728	1716	1360	255
80/20	1778	1728	1718	1362	258
50/50	1784	1737	1726	1369	266

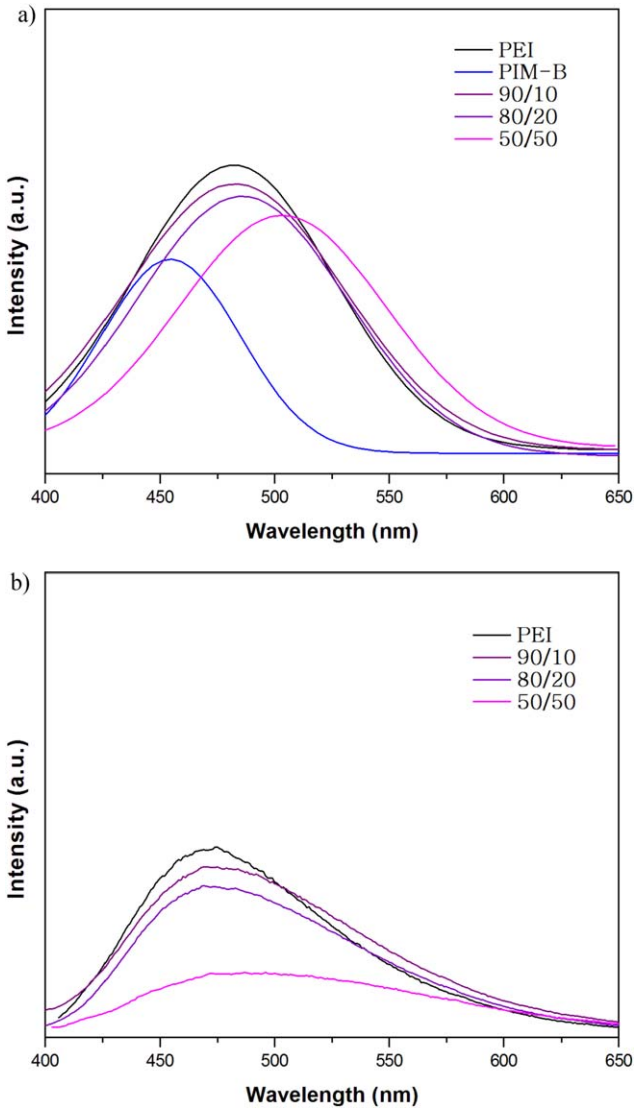

Figure 3. Emission spectrum of neat and blend membranes excited at (a) 222 nm and (b) 383 nm. [Color figure can be viewed at wileyonlinelibrary.com]

structures.[45] Thus, the characteristics of charge-transfer fluorescence in solid state polymers are spectral red-shift and fluorescence yield decrease when the excitation wavelength increases, meaning that the ability of the polymer to form charge transfer complexes increases.[17] In order to determine the existence of CTC, PI samples were excited at 222 and 383 nm due to samples showed fluorescent response at these wavelengths. Emission spectra are shown in Figure 3 (a,b). Membranes excited at 222 nm showed emission peaks at 482, 455, 483, 486, and 503 nm for neat PEI, PIM-B, 90/10, 80/20, and 50/50 membranes, respectively. When the polymeric membranes were excited at longer excitation wavelength (383 nm), fluorescence peaks of blend membranes red shifted to 488, 489 and 506 nm for 90/10, 80/20, and 50/50, respectively. Besides, these membranes showed a marked intensity decrease with respect to their emission bands at 222 nm. The intensity decrease was about 45, 49 and 77% for 90/10, 80/20, and 50/50 membranes, respectively.

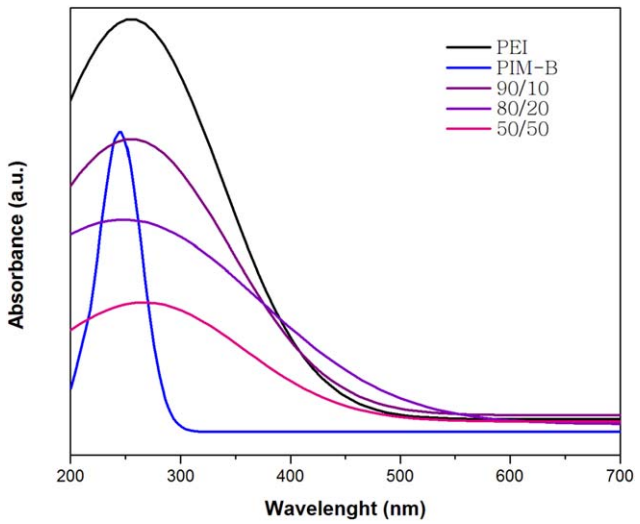

Figure 4. UV–vis absorption bands of PEI, PIM-B and the blend membranes. [Color figure can be viewed at wileyonlinelibrary.com]

This result indicates the intermolecular CTC formation increases as the amount of PIM-B increases in the blends. Furthermore, neat PEI also showed intensity decrease (42%) when it was excited at longer wavelength, however, no red-shift was observed for its fluorescent peak. On the contrary, microporous PIM-B did not show emission fluorescence at longer wavelength, meaning that intermolecular CTC are hindered in this polymer due to its contorted structure that prevents molecular packing.

Besides, if fluorescence peaks of blend membranes are compared to those of neat polyimides either for emission at 222 nm or 383 nm, it is observed a red-shift of the bands as the amount of PIM-B increases in the blend, being more pronounce for 50/50 membrane. Fluorescence analysis confirms FTIR results, showing the miscibility of PEI/PIM-B blends increases as the amount of microporous phase increases through intermolecular CTC formation. We can assume that at 50 wt % of PIM-B content, the contorted structure of neat PIM-B is modified to a more extended structure, due to molecular interactions which are responsible for a more efficient contact between PEI and PIM-B chains with respect to the other blend ratios.

UV–Vis Absorption

UV–vis spectrometry is a useful tool to analyze molecular interactions. Figure 4 and Table I show UV–vis absorption bands of PEI, PIM-B and the blends. Polymer membranes were prepared at thinner thicknesses (approx. 5 μm) in order to measure absorbance directly. Bands appeared in the region from 200 to 700 nm. Absorption bands centered at around 200 nm are associated with intramolecular charge–transfer interactions, while absorption bands in the range from 300 to 400 nm are related to intermolecular ones.[46] Furthermore, absorption tails above 350 nm, as well as, red-shift to higher wavelength (≥300 nm) confirm the presence of intermolecular charge–transfer complexes and their major extension with respect to intramolecular ones.[4,17,45] PEI showed a wide absorption band in the range from 200 to 450 nm, centered at 255 nm, approximately. The whole absorption band of PEI indicates charge–transfer complexes (CTC) may occur in the form of intramolecular and intermolecular CTC. PIM-B showed a narrower absorption band in a wavelength range from 200 to 300 nm. This result indicates that weak intramolecular interactions are present in PIM-B according to the contorted structured reported for FDA-6FDA microporous polyimide.[47,48] PEI/PIM-B blend membranes showed intensity decrease and absorption band red-shift as the amount of PIM-B increased. 90/10 blend membrane showed an absorption wavelength unaltered respect to neat PEI, that is, centered at the same wavelength (255 nm); however, it showed a marked intensity decrease which is attributed to the formation of intermolecular interactions. On the other hand, 80/20 blend membrane showed not only an intensity decrease but also a slight red shift of the absorption band towards higher wavelength (258 nm), between the values of neat PEI and PIM-B. Finally, 50/50 blend membrane showed a more pronounced shift towards higher wavelength (266 nm) superior to PEI and PIM-B absorption wavelength. These results evidenced that more CTC intermolecular interactions are formed as the amount of microporous phase increases. UV–vis absorption results were consistent with FTIR and fluorescence results which demonstrated that increasing PIM-B phase increase intermolecular interactions.

Opacity and Colorimetric Parameters

According to ASTM D1003 (ASTM, 2011) recommendations[38] and Gontard *et al.*[49] procedure film opacity was defined as the area under the recorded UV–vis curve determined by an integration procedure, that is, the opacity value is obtained indirectly through a transmission method. The opacity was expressed as Absorbance Units in nanometers (A.U. nm). Furthermore, colorimetric measurements using a Colorimeter MiniScan EZ model MSEZ-4500 L equipped with light source D65 and observation angle 10° were included for comparison. This colorimeter uses a CIE Lab system, in which color is represented by three dimensions: L^* related to lightness varied from black (zero) to white (100), and other two related to chromaticity, a* from green (−a*) to red (+a*) and b* from blue (−b*) to yellow (+ b*). Opacity can also be measured using this equipment through a direct measurement on the sample applying a reflection method. Measurements were taken at room temperature. L^*, a*, b* and OP values were averaged from three readings at each membrane. Results are presented in Table II.

Table II. Opacity and Colorimetric Measurements

Polymer	OP_1 (A.U. nm)	OP_2	L*	a*	b*
PEI	177	1.04	83.74	−1.41	2.46
PIM-B	59	0.55	93.45	−2.33	1.78
90/10	146	3.38	83.54	−0.64	2.55
80/20	127	9.15	77.60	−0.67	19.22
50/50	84	11.02	73.84	−0.68	27.95

OP_1 = obtained as [39, 52]; OP_2 = obtained through MiniScan EZ15 measurement.

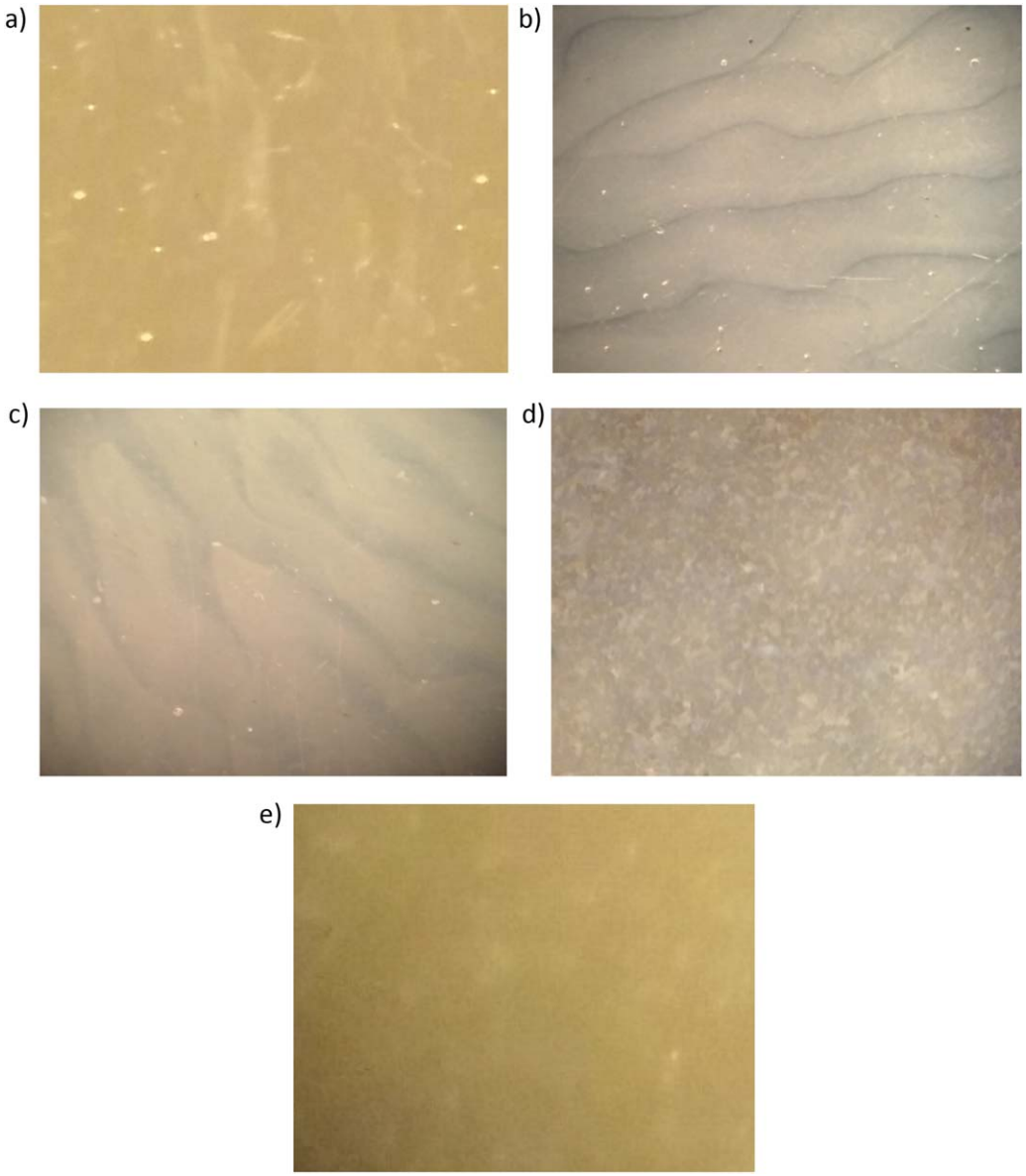

Figure 5. PLM images of (a) PEI; (b) 90/10; (c) 80/20; (d) 50/50; and (e) PIM-B. [Color figure can be viewed at wileyonlinelibrary.com]

According to OP_1 values, opacity decreases as the amount of PIM-B increases in the blends. Taking into account the referenced literature[5–9,38,49] about opaque materials indicate low miscibility, it might state that PEI/PIM-B membranes show higher miscibility as the amount of PIM-B increases in the blends. This result is consistent with FTIR, fluorescence spectroscopy, and UV–vis analysis and demonstrates that miscibility increases according to the increase in CTC interactions. On the contrary, colorimetric results showed an increase in OP_2 as well as a decrease in L^* as the amount of PIM-B increased in the blends. Ando *et al.*[50] studied the relationships between the color intensities of polyimide films and the electronic properties of their source materials (aromatic diamines and aromatic tetracarboxylic dianhydrides) and they concluded that higher intermolecular CTC formation was proved by a deeper coloration in polyimide films, with colors ranging from pale yellow to deep brown. Besides, they reported that bulky and weakly polarizable —$C(CF_3)_2$— groups prevent molecular packaging and lighten the color of polyimides rendering polymers with high optical transparency. According to these authors, it is reasonably to observe that neat PIM-B showed the lower opacity as well as higher luminosity, while blend membranes became more opaque as the amount of PIM-B increases in the blend. This is due to an increment in intermolecular CTC interactions, which were responsible for higher miscibility in the blends. The color of blend membranes changes from pale yellow to light brown as the amount of PIM-B increases in the blends, retaining the transparency of the membranes even when opacity increases. Photograph of all prepared membranes were included in the graphical abstract. Even though both analysis (OP_1 and OP_2) are contradictory in their tendencies, based on cited literature, it is demonstrated that miscibility is improved through

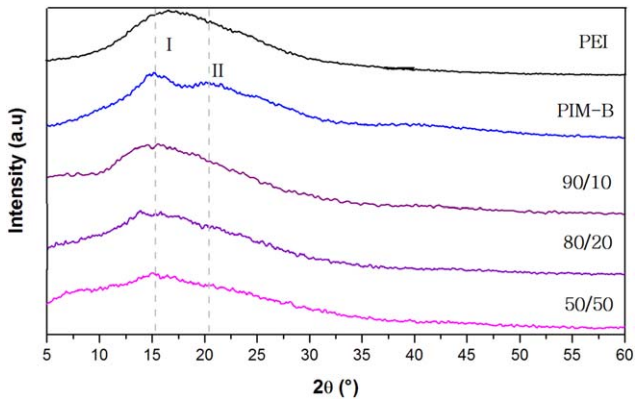

Figure 6. XRD of PEI, PIM-B and the blend membranes (dashes lines indicate I and II bands reported in Table III). [Color figure can be viewed at wileyonlinelibrary.com]

intermolecular CTC formation as the amount of PIM-B increases in the blend.

PLM Images Analysis

The miscibility of the PEI/PIM-B blends was studied through optical inspection of the membranes using a PLM microscope at ambient temperature. Images from Figure 5 were analyzed as a function of PIM-B content. Clear partial miscibility was observed as the amount of PIM-B increases in the blend. This result was proved by a change at the interface of the homopolymers from a defined interface to a diffuse interface as the amount of PIM-B increases from 10 to 20 wt %. Besides, at 50/50 blend ratio no interface was observed indicating an improved solubility of one polymer into the other. The interface becomes more diffuse as the miscibility increases due to the increment in intermolecular CTC. These results are consistent with FTIR, fluorescent, and UV–vis data, and they will be finally confirmed by x-ray diffraction (XRD) and DSC characterization techniques.

Wide-Angle X-ray Diffraction

Structures of PEI, PIM-B, and blend membranes were investigated through XRD analysis. XRD patterns of membranes showed broad halos in the 2θ range of 5–60°. The top of the broad peaks on each X-ray pattern was attributed to the intersegmental interference and it is representative of the average intersegmental distance named the mean interchain distance (d-spacing).[51,52] From Figure 6 and Table III, it is observed that all prepared membranes have amorphous XRD patterns. PEI presented the lowest d-spacing value with respect to all prepared membranes meaning that it has the densest packed structure. PIM-B showed a general amorphous structure with one narrower peak centered at 2θ = 15.2° and a wider amorphous band at 2θ = 20.2°. Similar 2θ angles were reported by Weber *et al.*[37] for PIM-B (FDA-6FDA) casting film. These 2θ angles indicate that PIM-B has two different ordered regions in solid state. The halo at higher angles is attributed to the chain-to-chain efficient packed regions and the halo at lower scattering angles to more loosely packed polymer chains, that is, to segments keeping their conformation with the micropores in between.[37] Blend membranes showed a decrease in d-spacing as the amount of microporous phase increased. Furthermore, it was observed that the d-spacing corresponding to Band II for neat PIM-B disappears in blend membranes, while the d-spacing having the microporous in between (Band I) shifts to lower d-spacing values. This result indicates that the more packed structure of neat PIM-B is modified by a chain-to-chain efficient packed structure of PEI-PIM-B, that is, blend membranes become more miscible as the amount of PIM-B increases.[47,48] XRD observations are in agreement all characterization techniques discussed before.

The major formation of CTC in blend membranes as the amount of PIM-B increases is favored by the kink angle of 9FDA monomer (~109°). Weber *et al.*[37] stated that a larger kink angle (~109° for 9FDA compared to ~77° for BINAM or ~90° for spiro compounds) leads to more elongated chains rather than highly contorted ones, which favors close packing and/or intercalation between polymer chains. Thus, XRD results are also in good agreement with FTIR, fluorescence, and UV–vis analysis.

Differential Scanning Calorimetry

DSC analysis of polymer blends allows knowing the occurrence of homogeneous or heterogeneous blending. Inhomogeneous blends of partially miscible or immiscible components present two glass transitions corresponding to neat polymers. In contrast, homogeneous blends are completely miscible and they exhibit only one single glass transition.[53,54] T_g values determined by DSC study are shown in Table III. Glass transition temperatures were taken at the inflection point of DSC curves after two scans. The second scan allows reaching a higher resolution of DSC curves. PEI showed a glass transition temperature at 215 °C. This result was similar to those reported by other authors.[55,56] Most of the polymers of intrinsic microporosity show no appreciable T_g value along the DSC curves[26,27,29]; however, PIM-B presented a T_g at 408 °C, value which was higher than those reported by other authors (358–380 °C).[36,57,58] DSC curves for PEI, PIM-B, and blend membranes were included in Supporting Information as Figures S3–S7, respectively.

Blend membranes depicted variation of T_g according to a composition-dependent behavior. When PIM-B content was 50 wt. % two Tgs at 218 and 386 °C were observed for PEI and PIM-B phases, respectively. Similarly, when the amount of PIM-B was 20 wt % Tgs at 217 and 322 °C appeared, while for 90/10 blend membrane only one single T_g at 216 °C related to the T_g

Table III. XRD Results and Thermal Behavior of Membranes

	d-spacing (Å)			
Polymer	Band I	Band II	T_g (°C)	T_d (°C)
PEI	5.32	—	215	566
PIM-B	5.84	4.39	408	543
90/10	5.80	—	216/n.a.	561
80/20	5.64	—	217/322	557
50/50	5.53	—	218/386	550

n.a. = no appear.

Table IV. Gas Permeability and Ideal Separation Factors ($\alpha_{i/j}$) ($T_c = 35°C$ y $p_1 = 5$ bar)

Polymer	P_{H2} Δε±4%	P_{O2} Δε±5%	P_{CO2} Δε±5%	$\alpha_{H2/CH4}$ Δε±11%	$\alpha_{H2/CO2}$ Δε±9%	$\alpha_{H2/N2}$ Δε±11%	$\alpha_{O2/N2}$ Δε±12%	$\alpha_{CO2/CH4}$ Δε±12%
PEI	6.90	0.38	1.56	238	4.42	133	7.31	54
PIM-B	110.41[a]	14.50[a]	70.44[a]	57[a]	1.57[a]	38[a]	5.02[a]	36[a]
90/10	8.66	0.50	1.86	185	4.66	127	7.27	40
80/20	14.11	0.97	1.63	271	8.66	159	10.90	31
50/50	15.89	1.78	3.01	31	5.28	68	7.60	6

P (B); 1 Barrer (B) = 10^{-10} (cm^3(STP)cm/cm^2 cmHg s); Δε(%) percentage error; a = Data taken from Ref. 57 at $T_c = 30°C$ and $p_1 = 1.08$ bar.

of PEI phase was observed. The increase in T_g value of PEI phase as well as the decrease in T_g value of PIM-B phase in the blend membranes evidenced an improved solubility of one polymer into the other as the amount of PIM-B increases, hence partially miscible blends were prepared. It is important to note that the absence of T_g corresponding to PIM-B phase in 90/10 blend membrane is due to the low percentage of this second phase within the blend, so it was difficult to be detected from this technique. Xue *et al.*[59] reported similar results about PTT/ABS blends. They showed that partially miscible blends were obtained due to a composition-dependent thermal behavior when the ABS content was increased. They concluded that miscibility of the PTT/ABS blends improved slightly as the ABS content increased, and the solubility of ABS in the PTT-phase was greater than that of PTT in ABS-phase. Taking into account our DSC results and the analysis made from PLM images we can conclude that (i) miscibility of PEI/PIM-B blends improved as the PIM-B content increased and (ii) a greater solubility of PIM-B in the PEI-phase was observed.

Besides, a degradation temperature (T_d) analysis was made and the results are shown in Table III and Figure S7 from Supporting Information. Degradation temperatures were obtained from the maximum of the DSC curves between 500 and 600 °C. PEI showed the highest T_d (566 °C) according to the more packed structure observed in XRD analysis. On the opposite, PIM-B showed the lowest T_d (543 °C) regarding to its contorted and less packed structure. This result again agrees with the highest d-spacing observed in XRD diffraction pattern of PIM-B (Band I in Table III). Finally, blend membranes depicted T_d values between those of neat polymers, showing a decrease in T_d as the amount of microporous phase increased. It is known that the stiffness of polymer chains is associated with higher T_g, while extended molecular interactions are associated with higher T_m (melting temperature) and T_d.[60] From Table III, it is clearly seen that the degradation behavior of blend membranes is highly influenced by the contorted structure of PIM-B rather than the increased molecular interactions in the blends.

Transport Properties

Pure gas permeation results of membranes are shown in Table IV and they were obtained averaging the values attained from three samples of each membrane. Preliminary permeation test of CO_2 plasticization effect on every polymer in the range of $p_1 = 1$–10 bar was made. Results indicated that the upstream gas pressure or gas concentration in the range of 3–10 bar had no significant effect on the gas permeabilities (see Figure S8, Supporting Information). From this analysis, the intermediate upstream pressure of $p_1 = 5$ bar was chosen in all the gas permeation studies. The individual gases were measured in the following order H_2, N_2, O_2, CH_4, and CO_2 in order to avoid the effects of plasticization. PEI gas permeation coefficients were similar to those reported in previous work.[31] Because of the difficult handling of the PIM-B membrane; we could not subject it to gas permeability tests. However, other authors have reported PIM-B permeabilities for H_2, N_2, O_2, CH_4, and CO_2 (see Table IV), and propylene–propane gases.[57,58] These dissimilar results might be due to differences in polymer synthesis and membrane preparation as well as cell permeation design. It is well-known that polymers of intrinsic microporosity exhibit extraordinary high gas permeabilities but low to moderate selectivities.[27,28,47] All blend membranes showed higher permeation coefficients than neat PEI, due to they have higher d-spacing according to XRD results. Besides, a linear increase of permeability as the amount of PIM-B increases was observed for all assayed gases with improvements in gas selectivity at certain blend ratios. Furthermore, focus on the gas permeability of blend membranes; it was observed that permeability increased as d-spacing of the blend membranes decreased. This result seems not to be coherent considering that lower d-spacing should cause decreasing of permeability. However, considering partially miscible PEI/PIM-B blends exhibit regions rich in densest packed phase, as well as, regions rich in microporous phase, it is assumed that a competition between chain packing, which improves as the amount of PIM-B increases, and intrinsic microporosity, which is not modified by blending, is affecting the permeability behavior. Similar results were reported by Chun *et al.*[57] who studied gas permeation properties of a series of three-component polyimides consisting of 6FDA-FDA-HFBAPP. These authors found that the higher the packing density, the higher the gas permeability was. Through XRD results these authors showed that an increasing FDA segment ratio creates an increasing "effective" free volume for gas permeation in the three-component polyimides. They attribute this behavior to the FDA segment is better ordered as well as better packed than HFBAPP segment. However, it keeps the same segmental distance. On the other hand, Chung *et al.*[1,29] have recently reported the preparation and gas permeation results of PIM-1/Matrimid and Ultem/PIM-1 blends along the range from 100/0 to 0/100 polymer ratios. In both cases, these authors found that the permeability of pure gases increased as the amount of PIM-1 increased in the blends, while gas selectivity decreased.

Table V. Diffusion and Solubility Coefficients ($T_c = 35°C$ y $p_1 = 5$ bar)

Polymer	D_{N2} Δε±9%	D_{O2} Δε±7%	D_{CH4} Δε±9%	D_{CO2} Δε±7%	S_{N2} Δε±16%	S_{O2} Δε±12%	S_{CH4} Δε±16%	S_{CO2} Δε±12%
PEI	0.38	1.63	0.14	1.29	0.14	0.23	0.20	1.21
PIM-B	—	—	—	—	—	—	—	—
90/10	0.44	1.17	0.24	0.34	0.16	0.43	0.20	5.52
80/20	0.47	1.72	0.27	0.19	0.19	0.57	0.19	8.52
50/50	1.36	5.61	1.01	2.26	0.17	0.32	0.50	1.33

$D = 10^{-8}$ ($cm^2\ s^{-1}$); $S = 10^{-2}$ (cm^3(STP)/cm^3 cmHg); Δε(%) percentage error.

Correlation between gas permeability and d-spacing of blend membranes was only made for Ultem/PIM1. Authors showed that Ultem/PIM 1 (10:90) had a lower d-spacing value than PIM-1, while Ultem/PIM 1 (90:10) had a larger d-spacing value than Ultem. They demonstrated the higher the d-spacing of blend, the higher the gas permeability was. Besides, authors highlighted that the decrease in Ultem/PIM-1 gas selectivity was minimum regarding to the impressive increase (around 2 times) in gas permeability when the polymer ratio was 80:20 (Ultem/PIM-1). Authors explained that an increase in fractional free volume (FFV) as the amount of PIM-1 increases was responsible for higher gas permeabilities. However, they mentioned that positive deviations in free volume from the linear additional rule at low PIM-1 loadings may be resulted from interface voids, while negative deviations observed at higher PIM-1 loadings may be due to the filling of Ultem molecules into PIM-1 pores. In this work, a marked increase in gas selectivity of H_2/CH_4, H_2/CO_2, H_2/N_2, and O_2/N_2 gas pairs was observed for 80/20 blend membrane. Among them, H_2/CO_2 and O_2/N_2 ideal separation factors were one of the highest values reported up to now.[61–63]

In order to analyze whether diffusivity or solubility might be responsible for membrane selectivity, values of D ($D = l^2/6t_{\downarrow}$) and S from D and P based on the solution-diffusion model ($S = P/D$) were calculated, and they are included in Table V. Because of hydrogen time lag values were too short to be measured accurately, D and S coefficients of H_2 were not calculated. Diffusion coefficients of blend membranes were higher than that of neat PEI and they increased as the amount of PIM-B increased. The increment in gas diffusivity of blend membranes over the neat PEI matrix was attributed to the low gas flux resistance of the increasing microporous phase. Interestingly, 80/20 blend membrane presented the lowest diffusion coefficients for CO_2. It is not expected considering the kinetic diameter of the gases ($\sigma_{kCO2} = 3.36$ Å $< \sigma_{kO2} = 3.46$ Å $< \sigma_{kN2} = 3.64$ Å $< \sigma_{kCH4} = 3.80$ Å) and the d-spacing of the membranes (PIM-B > 90/10 > 80/20 > 50/50 > PEI). The kinetic diameter, which corresponds more closely to the minimum diameter of the molecule, has a strong effect on the penetrant mobility. It is evident that the smaller the penetrant kinetic diameter is, the higher the penetrant mobility will be through the polymer gaps to reach a new site. Taking into account this, it is expected that the diffusion coefficient of CO_2 was higher than the other gases for any membrane. Besides, according to the d-spacing, it is expected that the CO_2 diffusion coefficient for 80/20 blend membrane was lower than that of 90/10, as well as higher than those of PEI and 50/50 membranes. However, this logical behavior was not observed and it was attributed to a preferential sorption of CO_2 at a blend ratio of 80/20 due to the

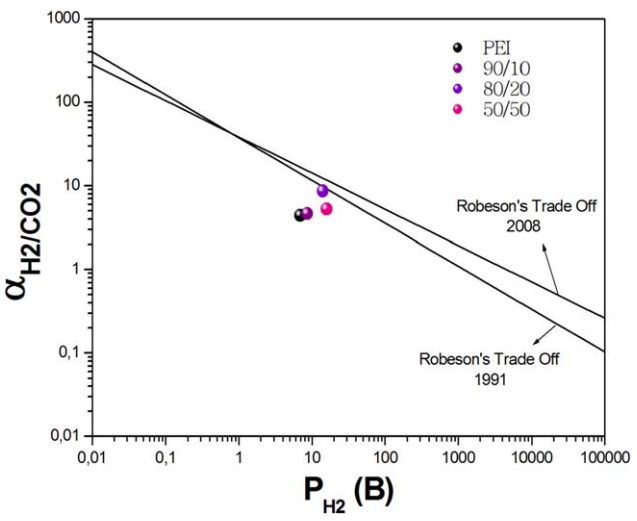

Figure 7. H_2/CO_2 Robeson Trade off and performance of membranes. [Color figure can be viewed at wileyonlinelibrary.com]

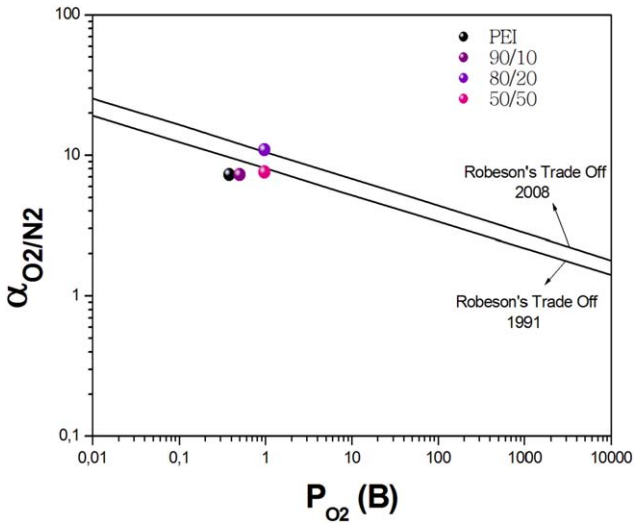

Figure 8. O_2/N_2 Robeson Trade off and performance of membranes. [Color figure can be viewed at wileyonlinelibrary.com]

presence of a wider and diffuse interface as it was shown in PLM images section. Table V also shows solubility coefficients of all membranes. It was observed, as a general tendency, an increase in gas solubility coefficients for blend membranes regarding to neat PEI. Interestingly, 80/20 blend membrane showed the highest CO_2solubility coefficient, while 50/50 blend membrane showed the lowest one. This result suggests that preferential gas sorption may occur not only at the microporous phase, but also at the interface of PEI/PIM-B partially miscible blend. Taking into account the observations made in PLM images; we assume that the wider and diffuse interface between PEI and PIM-B in 80/20 blend membrane favors the CO_2 sorption and increases its solubility. Taking into account that H_2 possesses the smallest kinetic diameter ($\sigma_{kH2} = 2.89$ Å) and its time lag was too short to be measured properly, it is assumed that H_2 present the highest diffusion coefficient with negligible solubility for any membrane. Therefore, in case of H_2 ideal separation factors, mobility selectivity ($D_{i/j}$) dominates the separation. The same apply for O_2/N_2 separation while, on the other hand, solubility selectivity ($S_{i/j}$) dominates the CO_2/CH_4 separation. Thus, extraordinarily high H_2/CO_2 and O_2/N_2 selectivities in 80/20 blend membrane is linked to the higher diffusion coefficient of smaller gas molecules such as H_2 and O_2 and the highest solubility coefficients of polar gas molecules such as CO_2. The structure of the 80/20 polymer matrix saturated by CO_2 sorption may retard a little the passage of the gas across the membrane due to the interaction between gas molecule and polymer segments.[64–66] Despite blend membrane at a ratio of 50/50 was proved to present stronger molecular interactions as well as lower d-spacing, typical high permeability and low selectivity of microporous phase predominated and consequently, it was responsible for the low gas separation performance of this membrane. Figures 7 and 8 depict upper bound graphics of Robeson for H_2/CO_2 and O_2/N_2, respectively. Both gas pairs are interesting to be separated at an industrial level due to the importance of their commercial use and purification.[2,67,68] The upper bound relationship for H_2/CO_2 was earlier published in 1994,[68] and since then not larger amount of data have been produced. Chung *et al.*[61] have recently reported a H_2/CO_2 separation factor of 7.3 for an ultraviolet (UV)-rearranged polymer of PIM-1. These authors attributed this high selectivity to the significantly enhanced diffusivity selectivity induced by UV radiation, followed by molecular rearrangement, conformational change and chain packing. In this work, an H_2/CO_2 separation factor of 8.66 was reached, placing the 80/20 blend membrane nearer to the attractive commercial region of Robeson graphics. Besides, this blend membrane also depicted an extraordinary high O_2/N_2 separation factor of 10.90, surpassing the 1991 and 2008 Robeson's upper bounds, and O_2/N_2 separation factors reported by other authors.[1,2,29,67]

CONCLUSIONS

Membranes prepared by blending PEI with PIM-B at different ratios combine good gas permeability with high selectivity for certain industrially important gas pairs. FTIR analysis as well as Fluorescence, UV–vis absorptions and optical properties showed formation of molecular interactions that favor blending. Thus, partially miscible blends were proved through the composition-dependent thermal behavior of the blends. XRD study showed structural changes when glassy polyetherimide and microporous polyimide were blended. Blend membranes showed a d-spacing between those of the homopolymers, which decreased as the amount of microporous phase increased from 10 to 50 wt % proving better molecular packing. However, the increment in gas permeabilities was driven by the increasing microporous phase in blend membranes. This behavior was attributed to a competition between chain packing and intrinsic microporosity. 80/20 blend membrane presented the best gas separation performance for most of the gas pairs analyzed. H_2/CO_2 and O_2/N_2 separation factors were dominated by mobility selectivity ($D_{i/j}$). However, high solubility of CO_2 ($S_{CO2} = 8.52 \times 10^{-2}$ cm^3(STP)/cm^3 cmHg) improved the separation performance of 80/20 blend membrane through a preferential sorption of CO_2 in the microporous phase and in the interface of PEI and PIM-B polymers. The structure of the 80/20 polymer matrix saturated by CO_2 sorption may retard the passage of the gas across the membrane and thus favors selectivity. Synergistic properties of PEI and PIM-B at a ratio of 80/20 resulted in extraordinarily high H_2/CO_2 and O_2/N_2 separation factors.

REFERENCES

1. Yong, W. F.; Li, F. Y.; Xiao, Y. C.; Li, P.; Pramoda, K. P.; Tong, Y. W.; Chung, T. S. *J. Membr. Sci.* **2012**, *407*, 47.
2. Robeson, L. M. *J. Membr. Sci.* **2008**, *320*, 390.
3. He, Y.; Zhu, B.; Inoue, Y. *Prog. Polym. Sci.* **2004**, *29*, 1021.
4. Sun, Z.; Li, H.; Zhuang, Y.; Ding, M.; Feng, Z. *Polym. Bull.* **1991**, *26*, 557.
5. Kim, C. K.; Paul, D. R. *Macromolecules.* **1992**, *25*, 3097.
6. Kelarakis, A.; Yoon, K. *Eur. Polym. J.* **2008**, *44*, 3941.
7. Im, H.; Kim, H.; Kim, J. *Mater. Trans.* **2009**, *50*, 1730.
8. Zhang, W.; Gui, Z.; Lu, C.; Cheng, S.; Cai, D.; Gao, Y. *Mater. Lett.* **2013**, *92*, 68.
9. Marwat, Z. K.; Baloch, M. K. *Eur. Polym. J.* **2015**, *66*, 520.
10. Ahn, T. K.; Kim, M.; Choe, S. *Macromolecules.* **1997**, *30*, 3369.
11. Rajagopalan, P. T.; Kandpal, L. D.; Tewary, A. D.; Singh, R. P.; Pandey, K. N.; Mathur, G. N. *J. Therm. Anal. Calorim.* **1997**, *49*, 143.
12. Ismail, A. F.; Rahim, R. A.; Rahman, W. A. *Sep. Purif. Technol.* **2008**, *63*, 200.
13. Kapantaidakis, G. C.; Koops, G. H.; Wessling, M. *Desalination.* **2002**, *145*, 353.
14. Wu, H. L.; Ma, M. C. C.; Li, C. H.; Lee, T. M.; Chen, C. Y.; Chiang, C. L.; Wu, C. *J. Membr. Sci.* **2006**, *280*, 501.
15. Ruvolo-Filho, A.; Barros, A. F. *Polym. Degrad. Stabil.* **2001**, *73*, 467.
16. Hudson, S. D.; Davis, D. D.; Lovinger, A. J. *Macromolecules.* **1992**, *25*, 1759.
17. García, M. G.; Marchese, J.; Ochoa, N. A. *Int. J. Hyd. Ener.* **2010**, *35*, 8983.
18. Harris, J. E.; Robeson, L. M. *J. Appl. Polym. Sci.* **1988**, *35*, 1877.

19. Weber, J.; Antonietti, M.; Thomas, A. *Macromolecules.* **2008**, *41*, 2880.
20. Budd, P. M.; Elabas, E. S.; Ghanem, B. S.; Makhseed, S.; Mckeown, N. B.; Msayib, K. J.; Tattershall, C. E.; Wang, D. *Adv. Mater.* **2004**, *16*, 456.
21. Budd, P. M.; Msayib, K. J.; Tattershall, C. E.; Ghanema, B. S.; Reynolds, K. J.; McKeown, N. B.; Fritsch, D. *J. Membr. Sci.* **2005**, *25*, 1263.
22. McDermott, A. G.; Larsen, G. S.; Budd, P. M.; Colina, C. M.; Runt, J. *Macromolecules.* **2011**, *44*, 14.
23. Ghanem, B. S.; McKeown, N. B.; Budd, P. M.; Selbie, J. D.; Fritsch, D. *Adv. Mater.* **2008**, *20*, 2766.
24. Ghanem, B. S.; McKeown, N. B.; Budd, P. M.; Al-Harbi, N. M.; Fritsch, D.; Heinrich, K.; Starannikova, L.; Tokarev, A.; Yampolskii, Y. *Macromolecules.* **2009**, *42*, 7881.
25. Ma, X.; Swaidan, R.; Belmabkhout, Y.; Zhu, Y.; Litwiller, E.; Jouiad, M.; Pinnau, I.; Han, Y. *Macromolecules.* **2012**, *45*, 3841.
26. Wang, Z.; Wang, D.; Jin, J. *Macromolecules.* **2014**, *47*, 7477.
27. Swaidan, R.; Ghanem, B.; Al-Saeedi, M.; Litwiller, E.; Pinnau, I. *Macromolecules.* **2014**, *47*, 7453.
28. Tocci, E.; De Lorenzo, L.; Bernardo, P.; Clarizia, G.; Bazzarelli, F.; Mckeown, N. B.; Carta, M.; Malpass-Evans, R.; Friess, K.; Pilnáček, K.; Lanč, M.; Yampolskii, Y. P.; Straranníkova, L.; Shantarovich, V.; Mauri, M.; Jansen, J. C. *Macromolecules.* **2014**, *47*, 7900.
29. Hao, L.; Li, P.; Chung, T.-S. *J. Membr. Sci.* **2014**, *453*, 614.
30. Chung, T.-S.; Xu, Z.-L. *J. Membr. Sci.* **1998**, *147*, 35.
31. García, M. G.; Marchese, J.; Ochoa, N. A. *J. Appl. Polym. Sci.* **2010**, *118*, 2417.
32. De Vu, Q.; Koros, W. J.; Miller, S. J. *J. Membr. Sci.* **2003**, *211*, 311.
33. Chung, T.-S.; Jiang, L. Y.; Li, Y.; Kulprathipanja, S. *Prog. Polym. Sci.* **2007**, *32*, 483.
34. Takahashi, S.; Paul, D. R. *Polymer.* **2006**, *47*, 7519.
35. Dudley, C. N.; Schöberl, B.; Sturgill, G. K.; Beckham, H. W.; Rezac, M. E. *J. Membr. Sci.* **2001**, *191*, 1.
36. Ritter, N.; Senkovska, I.; Kaskel, S.; Weber, J. *Macromolecules.* **2011**, *44*, 2025.
37. ASTM (**2011**). Standards American Society for Testing and Materials, D1003. Standard Test Method for Haze and Luminous Transmittance of Transparent Plastics. Philadelphia, USA.
38. Anson, M.; Marchese, J.; Garis, E.; Ochoa, N. A.; Pagliero, C. *J. Membr. Sci.* **2004**, *243*, 19.
39. García, M. G.; Marchese, J.; Ochoa, N. A. *J. Mater. Sci.* **2012**, *47*, 3064.
40. Cesteros, L. C.; Meaurio, E.; Katime, I. *Macromolecules.* **1993**, *26*, 2323.
41. Bharathikannan, R.; Chandramohan, A.; Kandhaswamy, M. A.; Chandrasekaran, J.; Renganathan, R.; Kandavelu, V. *Cryst. Res. Technol.* **2008**, *43*, 683.
42. Paraschuk, D. Y.; Elizarov, S. G.; Khodarev, A. N.; Shchegolikhin, A. N.; Arnautov, S. A.; Nechvolodova, E. M. *JETP Lett.* **2005**, *81*, 467.
43. Carturan, S.; Quaranta, A.; Negro, E.; Bonafini, M.; Maggioni, G.; Della Mea, G. *IEEE Sensors J.* **2006**, *6*, 1445.
44. Hasegawa, M.; Ishii, J.; Shindo, Y. *Macromolecules.* **1999**, *32*, 6111.
45. Hsu, S. C.; Whang, W. T.; Chao, C. S. *Thin Solid Films.* **2007**, *515*, 6943.
46. Hasegawa, M.; Kochi, M.; Mita, I.; Yokota, R. *Eur. Polym.* **1989**, *25*, 349.
47. Du, N.; Robertson, G. P.; Song, J.; Pinnau, I.; Thomas, S.; Guiver, M. D. *Macromolecules.* **2008**, *41*, 9656.
48. Nah, C.; Han, S. H.; Lee, J.-H.; Lee, M.-H.; Lim, S. D.; Rhee, J. M. *Composites: Part B.* **2004**, *35*, 125.
49. Gontard, N.; Guilbert, S.; Cuq, J. L. *J. Food Sci.* **1992**, *57*, 199.
50. Ando, S.; Matsuura, T.; Sasaki, S. *Polymer.* **1997**, *29*, 69.
51. Xu, Y.; Chen, C.; Li, J. *Chem. Eng. Sci.* **2007**, *62*, 2466.
52. Niyogi, S.; Adhikari, B. *Eur. Polym. J.* **2002**, *38*, 1237.
53. Kong, X.; Teng, F.; Tang, H.; Dong, L.; Feng, Z. *Polymer.* **1996**, *37*, 1751.
54. Hosseini, S. S.; Teoh, M. M.; Chung, T. S. *Polymer.* **2008**, *49*, 1594.
55. Rezac, M. E.; Schöberl, B. *J. Membr. Sci.* **1999**, *156*, 211.
56. Pinto, B. P.; Santa Maria, L. C.; Sena, M. E. *Mat. Lett.* **2007**, *61*, 2540.
57. Chun, B.-W.; Ishizu, C.; Itatani, H.; Haraya, K.; Shindo, Y. *J. Polym. Sci. B Polym. Phys.* **1994**, *32*, 1009.
58. Shimazu, A.; Miyazaki, T.; Maeda, M.; Ikeda, K. *J. Polym. Sci.: Part B: Polym. Phys.* **2000**, *38*, 2525.
59. Xue, M.-L.; Yu, Y.-L.; Chuah, H. H.; Rhee, J. M.; Kim, N. H.; Lee, J. H. *Eur. Polym. J.* **2007**, *43*, 3826.
60. Billmeyer, F. W. Jr. Textbook of Polymer Science, 2nd ed.; Wiley Interscience, New York, **1971**.
61. Li, F. Y.; Xiao, Y.; Ong, Y. K.; Chung, T. -S. *Adv. Energy Mater.* **2012**, *2*, 1456.
62. Rangel, E. R.; Maya, E. M.; Sánchez, F.; de Abajo, J.; de la Campa, J. G. *J. Membr. Sci.* **2013**, *447*, 403.
63. Kim, Y.-H.; Kim, H.-S.; Kwon, S.-K. *Macromolecules.* **2005**, *38*, 7950.
64. Park, S.-H.; Kim, K.-J.; So, W.-W.; Moon, S.-J.; Lee, S.-B. *Macromol. Res.* **2003**, *11*, 157.
65. Weber, J.; Su, Q.; Antonietti, M.; Thomas, A. *Macromol. Rapid Commun.* **2007**, *28*, 1871.
66. Pandiyan, S.; Brown, D.; Neyertz, S.; Van der Vegt, N. F. A. *Macromolecules.* **2010**, *43*, 2605.
67. Robeson, L. M. *J. Membr. Sci.* **1991**, *62*, 165.
68. Robeson, L. M.; Burgoyne, W. F.; Langsam, M.; Savoca, A. C.; Tien, C. F. *Polymer.* **1994**, *35*, 4970.